metals

Article

Theoretical Study of Asymmetric Bending Force on Metal Deformation in Cold Rolling

Zhuwen Yan, Shuaizhen Pan *, Yingxin Tang and Wenjun Cao

Jiangsu Provincial Engineering Laboratory of Intelligent Manufacturing Equipment, Industrial Technology Research Institute of Intelligent Equipment, Nanjing Institute of Technology, Nanjing 211167, China; yan-zhuwen@njit.edu.cn (Z.Y.); njtangyingxin@outlook.com (Y.T.); cwj7192@163.com (W.C.)
* Correspondence: panshuaizhen1101@163.com

Abstract: A three-dimensional elastic–plastic finite element model of a six-roll cold rolling mill has been developed using the finite element software ABAQUS. The actual parameters of the rolling mill have been incorporated into the finite element model, with the working conditions applied as boundary constraints and load conditions. Subsequently, a non-symmetrical bending force is introduced to the finite element model. Through simulation calculations, this study analyzes the patterns of change in the transverse pressure of the rolling mill and roller pressure during non-symmetrical bending, as well as the variations in strip thickness, crown, edge drop, and flatness. Additionally, the regulating function of the bending force is examined. Each adjustment of 5 t in the asymmetric bending force results in an increase of approximately 0.01 mm in the thickness of the positive bending side of the strip while causing a decrease of about 0.01 mm in the thickness of the negative bending side. Therefore, the application of asymmetric bending forces proves to be effective in controlling the shape of lateral wave defects on the edges of steel strips.

Keywords: asymmetrical bending force; flatness; strip; finite element

Citation: Yan, Z.; Pan, S.; Tang, Y.; Cao, W. Theoretical Study of Asymmetric Bending Force on Metal Deformation in Cold Rolling. *Metals* **2024**, *14*, 1168. https://doi.org/10.3390/met14101168

Academic Editor: José Valdemar Fernandes

Received: 5 September 2024
Revised: 6 October 2024
Accepted: 10 October 2024
Published: 13 October 2024

1. Introduction

High precision in controlling board shape is a common objective for workers in the rolling process and is crucial for enhancing the quality of strip rolling technology. Modern cold rolling machines often employ various plate-shape control techniques, including roll tilting [1], cross-rolling [2,3], segmented cooling control [4], and bending rolls [5,6].

To investigate the impact of these controls on shape, an effective and precise calculation method for rolling is essential. Since the inception of rolling technology, a range of analytical and numerical methods have been utilized for rolling calculations. Traditional computational methods include the elastic beam method [7], influence function method [8], plate method [9], and boundary element method [10], among others. In comparison to these methods, the finite element method [11–16] stands out as a practical and powerful tool for computation.

In recent years, an increasing number of scholars have employed the finite element method to develop rolling models. Wang et al. [17] established a two-dimensional finite element model to examine the effects of various factors, including the width of the steel strip, rolling force, bending force, roll convexity, and roller diameter, on the convexity of the steel strip. However, models created using two-dimensional finite element software typically represent flat rolls, which differ significantly from actual rollers, leading to reduced accuracy. Li et al. [18] further advanced this research by developing a half-cylindrical roller model based on a three-dimensional finite element framework, investigating the impact of edge cooling on the shape and flatness of the steel strip. The use of a one-half model can enhance computational efficiency; however, it significantly reduces data reliability and accuracy. Consequently, some researchers have started to develop finite element models based on dynamic principles. When employing the implicit method for computation, each iteration necessitates solving a substantial number of linear equations, which results in decreased computational efficiency and a higher likelihood of divergence.

Therefore, most contemporary researchers employ explicit dynamic methods to develop rolling models [19–22]. Wang et al. [23] utilized the explicit dynamics method to create a finite element model, investigating the impact of horizontal shift control of work rolls on the edge drop in six-roll cold rolling mills. They analyzed the modeling process, highlighting the advantages of the explicit dynamics method, including excellent convergence, high stability, accuracy, and efficiency. Yu et al. [24] and Pan et al. [25] applied the explicit dynamics finite element software LS-DYNA 970 to simulate the 3-pass and 16-pass hot-rolling processes, respectively, and innovatively developed geometric modeling techniques. Wang et al. [26] created a hot-rolled strip flatness analysis model that incorporates lateral metal flow and established a three-dimensional finite element model using the explicit dynamics method, confirming the model's reliability. Utilizing the finite element method (FEM), Kapil S. et al. [27] formulated the equation governing the motion of the working roll in a four-high rolling mill setup. This model facilitates the prediction of the final strip's profile shape and the variation in exit stress, which is crucial for preventing common rolling defects, such as edge and center buckling. Dasari SK et al. [28] employed numerical simulation through finite element analysis (FEA) to accurately predict the softening phenomena occurring during the hot rolling process. By integrating this methodology, they significantly advanced the understanding and control of material behavior under high-temperature and deformation conditions. Sabar SK et al. [29] focused on applying finite element method (FEM) software strategies to forecast the rolling force (RF) in hot rolling processes, emphasizing the integration of nano-lubrication conditions. The aforementioned studies demonstrate that the finite element models developed using the explicit dynamics method exhibit high accuracy and reliability. Consequently, this paper adopts the explicit dynamics module of the ABAQUS 2023 simulation software for rolling simulations.

The common types of roll bending technology include support roll bending, working roll bending [30], and intermediate roll bending. The traditional control methods for these rolls primarily involve symmetric roll bending controls [31–34]. Shi et al. [35] applied the finite element software MARC 2005 to simulate the four-roll milling process of steel strips and found that the symmetric bending force significantly impacts board convexity. As the positive bending force increases, the thickness of the central region of the strip gradually increases, while there is minimal change in the edge reduction zone, and a decrease is observed in the abrupt reduction zone. Building on this, Ma et al. [36] utilized the finite element software ANSYS 7.0 to couple the relationship between the rolled piece and the roller, establishing a rolling model. The results indicated that while the bending force can enhance the symmetry of bilateral edge waves, excessive bending force may lead to increased machine power consumption and roller wear, with only marginal improvements in board shape. However, symmetric bending control is limited to regulating symmetric second and fourth board shape defects and cannot address non-symmetric board shape defects. To tackle the issue of asymmetric strip shapes, various researchers have developed methods for asymmetric bending roll control. Liu et al. [37] employed the influence function model to analyze the strip exit thickness, roll force distribution, and tension distribution following asymmetric bending control. Their findings revealed that asymmetric bending rolls can alleviate the unbalanced distribution of roll forces and, in certain cases, may even reduce the need for some roll tilt control. Hu et al. [38] used ANSYS software to simulate and analyze the force dynamics of the roll system under both positive and negative bending rolls. Additionally, Liu et al. [39] established a rolling model using ANSYS to determine the shape of the work roll and the bearing roll gap. Their results indicated that a four-roll mill equipped with asymmetric bending rolls could effectively address the challenge of weak control over the bearing roll gap's opening degree at various points along the full width of the board, thereby enhancing the mill's ability to control the board's flatness. While the aforementioned studies analyzed the impact of asymmetric bending rolls on strip thickness, pressure distribution between rolls, and the shape of the bearing roll gap [40,41], they did not further investigate the effects of asymmetric bending rolls on critical shape parameters such as crown, edge drop, and flatness.

This article primarily investigates the optimal conditions for strip steel rolling. A higher friction coefficient between the rolls indicates an increased degree of roll wear. In this study, roll wear is addressed by establishing an appropriate friction coefficient. To ensure the numerical analysis has broad applicability, a 1580 mm conventional six-high rolling mill from a specific steel rolling plant is utilized as a model, which is widely employed across various sizes of steel rolling mills. C40 steel (DIN EN ISO 683-1:2018) [42] is selected as the strip material due to its excellent plasticity and toughness, making it widely used in machinery manufacturing, construction, and the aviation industry. Given the selection of the most commonly used rolling mill and strip material, the numerical results and patterns derived can provide a comprehensive theoretical foundation for subsequent rolling experiments and manufacturing processes.

This paper utilizes ABAQUS simulation software to develop a model of asymmetrical bending rolls and analyze key shape parameters, including strip transverse thickness, roller pressure, rolling force, crown, and flatness based on the results obtained. Furthermore, it evaluates the regulatory effectiveness of bending forces to assess their capability in controlling strip shape.

2. Establishing Finite Element Simulation

2.1. Scenario Selection

To accurately determine the deformation behavior of steel strips, a high-precision finite element model is essential. Consequently, ABAQUS software is employed to develop the simulation model. ABAQUS offers two solvers: the implicit dynamic method [43] (ABAQUS/Standard) and the explicit dynamic method [44] (ABAQUS/Explicit). The rolling process of steel strips presents a nonlinear quasistatic challenge characterized by complex contact conditions and substantial deformations. Utilizing the implicit method necessitates extensive computational resources and the resolution of numerous linear equations at each iteration, which can lead to low computational efficiency and potential divergence. Therefore, the explicit dynamic method is adopted to effectively simulate the rolling process of steel strips.

2.2. Parts and Materials

The model is divided into seven components, consisting of six rolls and one strip of steel. The roll bodies and necks are designed as integrated models to more accurately simulate the integrated casting of rolls. The geometric parameters of the rolls and strips are presented in Table 1. The foundation for investigating the impact of varying bending forces on the shape change in the strip lies in studying the variations in strip thickness and roll gap. Since the rolls exhibit elastic behavior during the rolling process, they cannot be treated as rigid bodies. Therefore, the six rolls are modeled as elastic bodies, while the strips, which undergo plastic deformation during rolling, are modeled as elastic-plastic bodies. Table 1 details the parameters for the various components of a six-high rolling mill.

The densities and elastic properties of the rolls [45] and strips [46] are identical, with a density of 7.85 g/cm^3, Young's modulus of 210,000 MPa, and a Poisson's ratio of 0.3. Additionally, the plasticity characteristics of the strips are described by the Johnson–Cook model, which consists of three primary components that represent strain hardening, strain rate strengthening, and thermal softening of the material. This model comprehensively accounts for the relationships among flow stress, strain, strain rate, and temperature, effectively addressing the requirements for simulating materials under various conditions.

The mathematical expression of the Johnson–Cook plasticity model [47] is as follows:

$$\sigma = (A + B\varepsilon^n)(1 + C\ln\frac{\dot{\varepsilon}}{\dot{\varepsilon_0}})(1 - [\frac{T - T_r}{T_m - T_r}]^m) \quad (1)$$

In the equation, A is the initial yield stress, in units of pressure. B is the hardening constant, also in units of pressure. n is the coefficient of strain rate sensitivity. The value of n determines the direction of plastic flow and the material model:

1. When $n = 1$, the material behaves as an ideal linear elastic material;
2. When $n = 0$, the material behaves as a nonlinear elastic material;
3. When $0 < n < 1$, the material behaves as a plasticity-dominant material.

Table 1. Geometry of parts of the model.

Component	Size
Rolled product cross-sectional dimension	38 mm × 1200 mm
Work roll diameter	760 mm
Work roll neck diameter	510 mm
Intermediate roll body diameter	840 mm
Intermediate roll neck diameter	740 mm
Supporting roll body diameter	1520 mm
Supporting roll neck diameter	1000 mm
Roll body length	1580 mm
Roll neck length	100 mm
Steel strip biting thickness	27.5 mm
Piece length	500 mm

c and m are dimensionless model parameters related to the strain rate and thermal softening effects. $T* = (T - T_r)/(T_m - T_r)$ is a dimensionless temperature, where T_r and T_m are reference temperatures, and T is the current temperature, while ε is the strain rate. Strip materials utilize C40 steel (DIN EN ISO 683-1:2018), and the five primary parameters of the Johnson-Cook model for C40 steel are presented in Table 2.

Table 2. Five parameters of the Johnson–Cook model of C40 steel (Adapted from Refs. [48,49]).

Parameter	Numeric Value
A	10.487
B	178.63
C	0.08139
n	0.25644
m	0.68196

2.3. Solution to Improve Computational Efficiency

The rolling direction, width direction, and thickness direction of the strip steel establish the spatial coordinates X, Y, and Z, respectively. Unlike scenarios where symmetric control shapes are employed, this article also examines the effects of asymmetric bending rolls on shape. Consequently, it is not feasible to utilize a half model based on symmetry about the XY plane to enhance computational efficiency.

Since an explicit central difference method is employed to solve dynamic equations, the discrete mass matrix significantly influences both computational efficiency and accuracy. When the mass scaling method is applied appropriately, it is possible to maintain computational accuracy while substantially enhancing computational efficiency. In slow-speed rolling, the rolling process of strip steel is typically regarded as a quasi-static process. Given that the stiffness and mass of all components in the model are uniform, the mass scaling method for static analysis can be applied to the entire model. Under any circumstances, there is no need to reduce the actual mass of the model, and arbitrarily increasing the mass will generally compromise computational accuracy. This article utilizes semi-automatic mass scaling, adjusting the time increment in ABAQUS/Explicit to 1×10^{-7} s, thereby reducing computation time and improving computational efficiency.

2.4. Rolling Conditions

The roller body and neck are flexible, altering in shape and size during motion. Therefore, directly driving the flexible body necessitates careful consideration of the forces and torques resulting from deformation and transformation, which adds complexity to the process. Additionally, in practical applications, the bearing drives the neck to transmit the motor's torque to the roller. To facilitate this, twelve rigid small cylinders are evenly distributed along each neck. The twelve rigid small cylinders are configured as rigid bodies, simulating fixed rollers and restricting their rotation. The rotational speed around the Z-axis for these rigid small cylinders is set to 5 revolutions per second, while the other five degrees of freedom are constrained. To ensure the strip is smoothly fed into the rolls, the initial speed in the X-direction is set to 1900 mm/s, matching the linear speed of the work rolls. In the explicit dynamic analysis, the penalty function method is employed for contact calculations, utilizing the "face-to-surface" interaction feature. The Coulomb friction coefficient between the strip and the rolls is set to 0.3.After the strip is bitten by the rolls, it advances in the direction of the rolling force due to the action of friction. Therefore, the strip is allowed to move freely in the X, Y, and Z directions, while its rotational freedoms are restricted to zero. To achieve a better shape in actual production, a tensile stress of 0.1 MPa is applied to the front surface of the strip, and a compressive stress of 0.08 MPa is applied to the rear surface.

2.5. Mesh Division

The accuracy and computational efficiency of a finite element model are significantly influenced by the mesh division. The types of grid elements include first-order tetrahedra, second-order tetrahedra, first-order hexahedra, and second-order hexahedra. The number of nodes for each type of element is 4, 8, 10, and 20, respectively. Generally, a higher number of nodes leads to more accurate results; however, it also decreases computational efficiency. Consequently, first-order tetrahedral and second-order hexahedral grids are typically not employed in standard calculations.

First-order hexahedral grids feature fewer elements and greater computational efficiency; however, obtaining rational grids for cylindrical models is more challenging, often necessitating complex model partitioning to achieve satisfactory grids. In contrast, second-order tetrahedral grids contain more elements, which increases computational time but also improves computational accuracy and ensures a more uniform distribution of the grid.

This paper employs a second-order tetrahedral element division while treating the rigid small circle as a solid with no deformation, which is represented as a hexahedral element. To balance accuracy and efficiency, the mesh utilizes a manual local division method. The mesh density is highest around the steel strip, followed by the surface of the roller, with the edges of the roller exhibiting the coarsest mesh. The total number of elements after division is 1,616,274. Figure 1 is the Roller edge mesh gradation schematic.

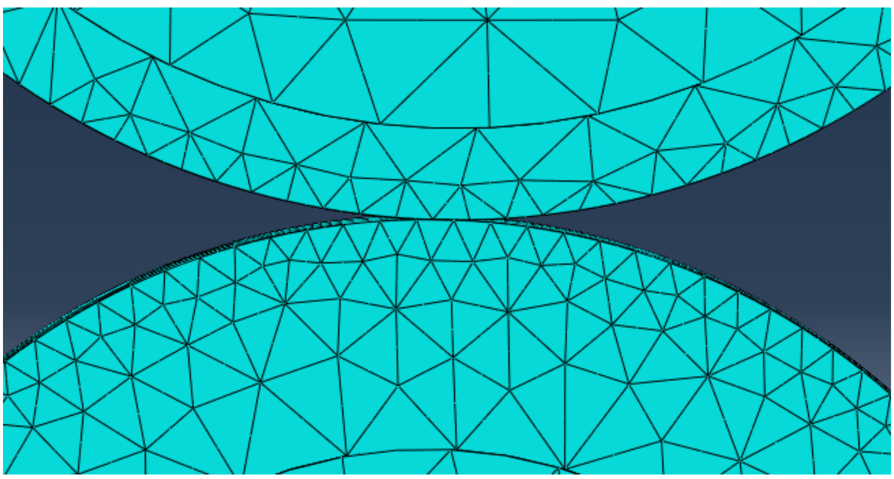

Figure 1. Roller edge mesh gradation schematic.

3. Simulation Results

The width of the simulation board for the rolling of strip steel is 1200 mm, and the explicit dynamics module of ABAQUS is utilized. Figure 2 is the stress diagram of the model. The control effect on the plate shape is most significant when applying bending forces to the working rolls; therefore, non-symmetric bending forces are applied at both ends of the working rolls. The bending force on the operational side is opposite to that on the transmission side, while the upper and lower work rolls experience the same force. The specific distribution of the roll bending force is illustrated in Figure 3. The bending force applied to the neck surface of the working roller is typically expressed in kilonewtons (kN), whereas in finite element analysis, it is represented as surface pressure, measured in megapascals (MPa). According to the mechanical formula, an increase of 1 MPa in surface pressure corresponds to a change of 10.2 kN in bending force. To minimize errors caused by unit conversion and to facilitate subsequent calculations, the bending force in this paper is expressed in MPa. After completing the rolling simulation with various roll bending forces, 61 nodes are selected on both the top and bottom surfaces of the strip. The thickness distribution along the horizontal direction of the strip is determined by subtracting the coordinates of the bottom nodes from those of the top nodes. Subsequently, the flatness, crown, and other shape assessment criteria of the strip are analyzed, and the regulatory effects of different roll bending forces are further investigated. For clarity in all illustrations, the left side represents the operating side, the right side represents the transmission side, and "left-right" refers to the horizontal distance between the operating and transmission sides of the strip.

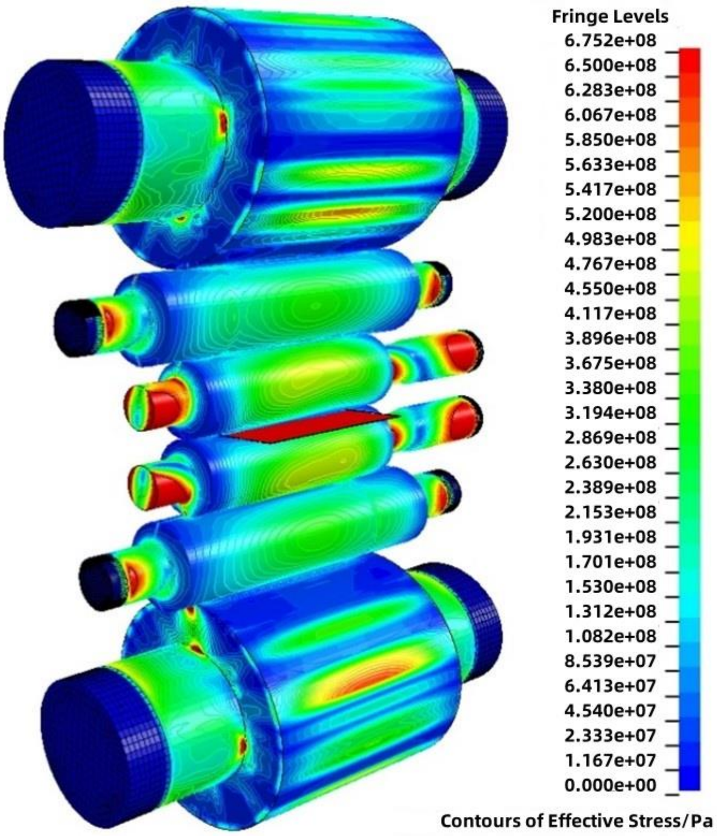

Figure 2. Contours of effective stress (maximum stress: 675 MPa, minimum stress: 12 MPa).

Figure 3. Asymmetric roll bending force schematic.

3.1. The Impact of Asymmetric Roll Forces on Equalizing Forces

The equivalent force diagrams for various conditions are presented in Figures 4–6. By analyzing these diagrams, it can be concluded that the concentrated region of equivalent force is situated 180 mm from the edge of the strip and exhibits left–right symmetry. Following the application of non-symmetric bending rolls, the concentrated area of equivalent force on the positive bending roll side decreases while the area on the negative bending roll side increases. This observation corresponds with the distribution pattern of rolling pressure discussed in the subsequent section.

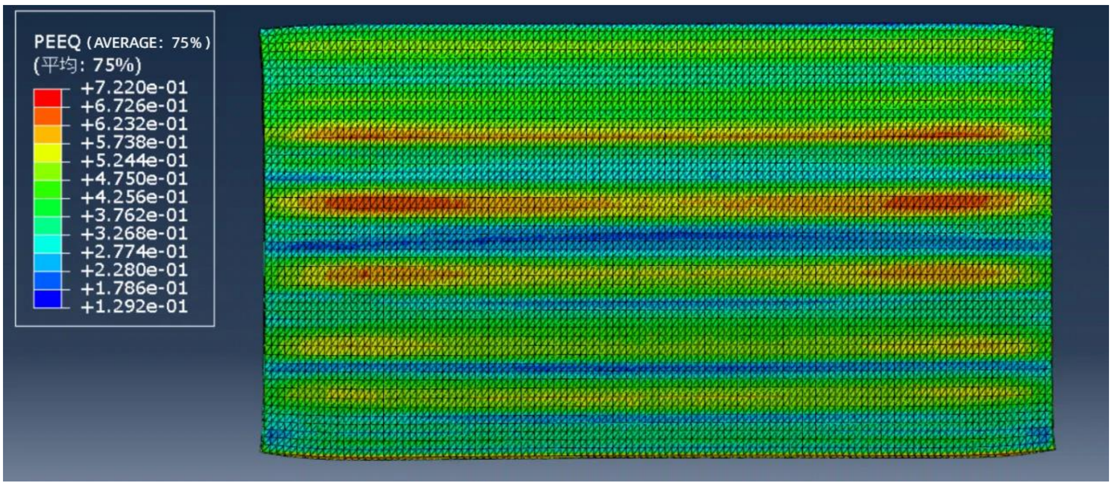

Figure 4. The equalizing force diagram without bending roller force.

3.2. The Impact of Asymmetric Bending Force on Rolling Pressure

Since the data and conclusions presented in this article are based on finite element simulations, we conducted experiments on rolling force under conditions identical to those in the simulations (i.e., without any bending force) to enhance the reliability of our findings. Figure 7 displays both the experimental rolling force curve and the simulated rolling force curve. The experimental results indicate that the simulated rolling force curve closely aligns with the experimental curve, with a maximum error of approximately 3%. Therefore, the precision of the finite element method described in this study meets the required standards.

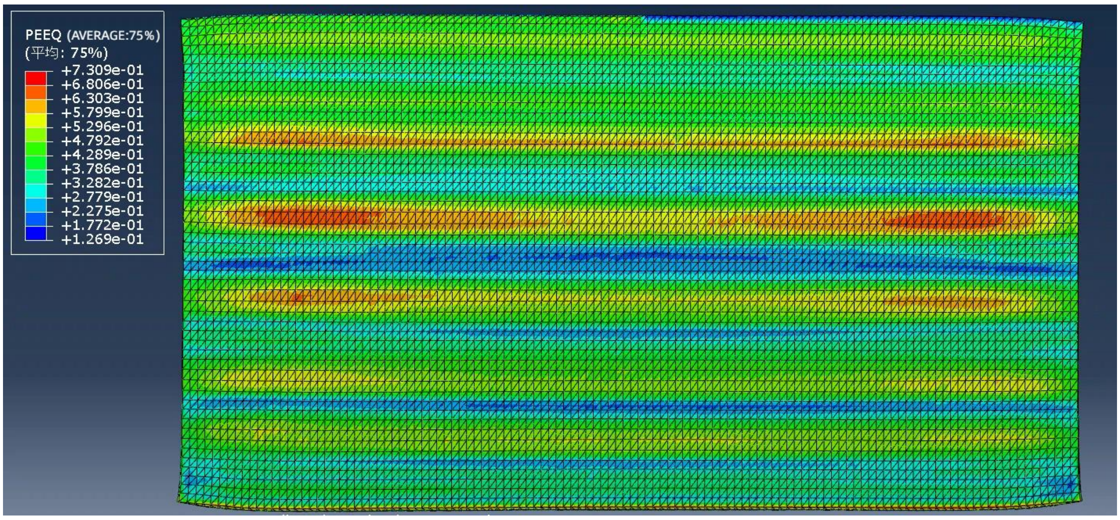

Figure 5. The equalizing force diagram with left negative bending roller force and right positive bending roller force.

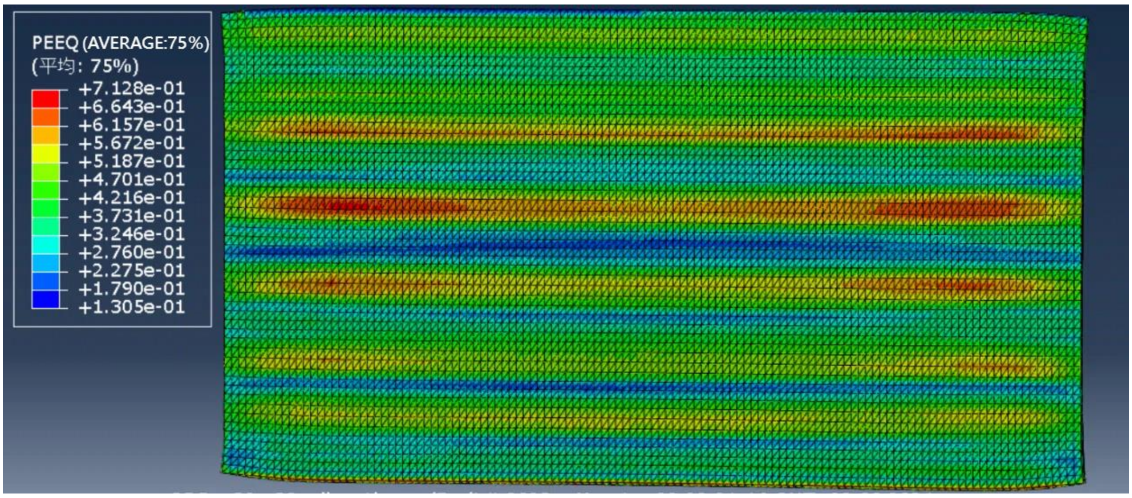

Figure 6. The equalizing force diagram with left positive bending roller force and right negative bending roller force.

Figures 8 and 9 illustrate the distribution curves of rolling pressure in the horizontal direction for cold-rolled strips subjected to various non-symmetrical roller forces. An analysis of Figure 8 indicates that within approximately 400 mm from the center of the strip, the distribution curve of the rolling pressure exhibits a parabolic shape, with a minimum value of about 180 MPa at the center and a maximum value of approximately 225 MPa at 400 mm from the center. In the range of 200 mm from the edge of the strip, the rolling pressure decreases linearly, dropping rapidly to around 115 MPa. By combining the analyses of Figures 8 and 9, it is evident that the rolling force undergoes asymmetric changes when subjected to non-symmetrical roller pressure. The rolling pressure on the side experiencing negative roller pressure increases slightly; however, this change is relatively minor, particularly within the 200 mm range from the edge, where the rolling pressure remains nearly constant. In contrast, the variation in rolling pressure on the side of the positive bending roller is significant. As the positive bending force increases, a clear trend of decreasing rolling pressure is observed. It is apparent that adjusting the non-symmetrical bending force is akin to modifying the rolling pressure at both ends of the mill, resulting in alterations to the thickness and shape of the steel strip.

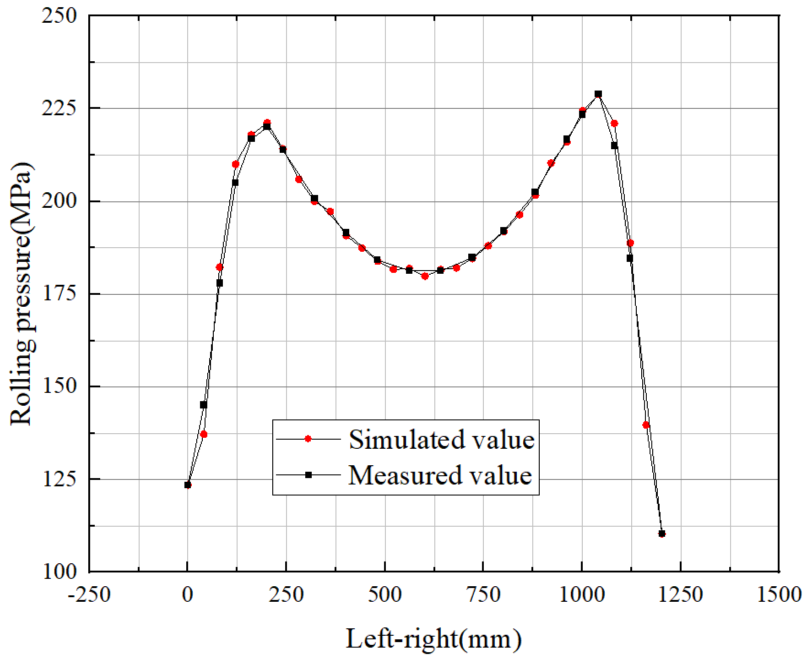

Figure 7. Comparison of measured values and actual values.

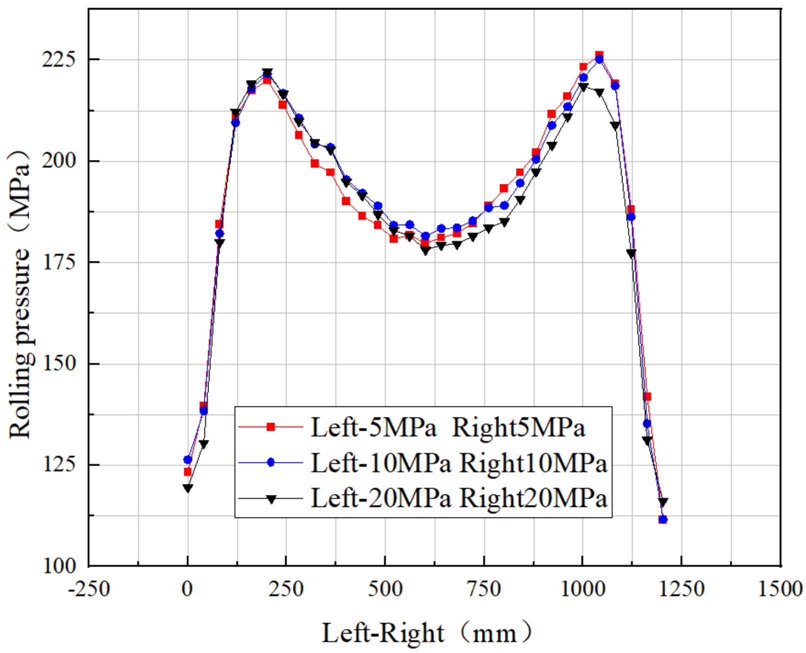

Figure 8. Diagram of the transverse distribution of rolling pressure with negative bending roll on the operating side and positive bending roll on the drive side.

3.3. The Impact of Asymmetric Roll Force on Inter-Roll Pressure

The distribution of inter-roll pressure across the working rolls and intermediate rolls at various levels of bending force is illustrated in Figure 10. In the absence of a bending force, the maximum inter-roll pressure reaches approximately 475 MPa at the center of the rolling mill and gradually decreases to about 60 MPa as one moves away from the center. When a non-symmetrical bending force of 30 MPa is applied to both sides of the working rolls, the change in inter-roll pressure at the center of the rolling mill is relatively minor. The pressure between the work rolls varies significantly within a 300 mm range from the edge of the roller, specifically increasing on the side where the positive bending force is applied and decreasing on the side where the negative bending force is exerted, resulting in asymmetric changes in roll gap pressure. As the non-symmetrical bending force continues to increase to 60 MPa, the behavior of the working roll resembles that of tilted rollers, with the pressure between the rolls in the middle section decreasing by approximately 50 MPa. The working and intermediate rolls on the positive bending force side compress each other, leading to an increase in roll gap pressure. The pressure between the rolls gradually flattens as it approaches the center of the roll at a distance of 700 mm. In contrast, there is a significant drop in pressure between the rolls in the area near the edge of the roll, approximately 100 mm from the center. Consequently, the pressure between the rolls on the negative bending force side decreases, with the pressure at the very edge of the roll dropping from 60 MPa to 0 MPa.

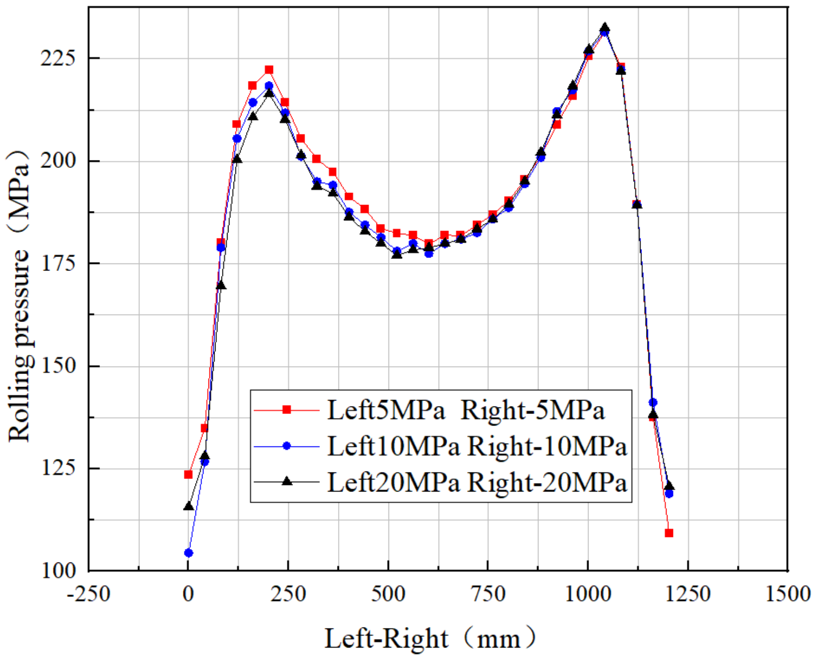

Figure 9. Diagram of the transverse distribution of rolling pressure with positive bending roll on the operating side and negative bending roll on the drive side.

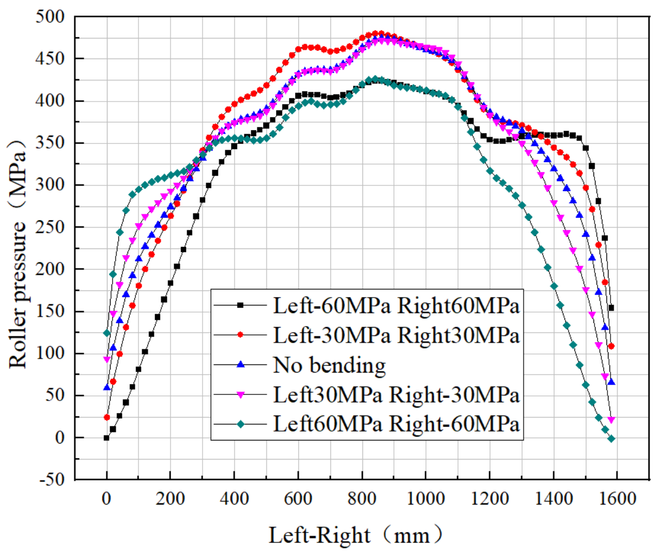

Figure 10. Horizontal distribution chart of working and intermediate roller pressures.

Figure 11 illustrates the distribution of pressure between the working and intermediate rolls under varying bending forces. In the absence of bending forces, the rolling pressure fluctuates continuously, with the supporting and intermediate rolls adjusting in real time to balance the overall interaction force between the rolls. This results in an unbalanced roll gap, where the operating side experiences higher pressure than the transmission side. As depicted in Figure 11, the application of negative and positive bending forces on the operating and transmission sides, respectively, alleviates the imbalance in roller pressure. The region between 0 and 200 mm on the operating side shows a slight reduction in roller pressure, while the area between 200 and 1580 mm on the transmission side exhibits a significant increase in roller pressure, averaging 25 MPa at a non-symmetric bending force of 30 MPa. The maximum roller pressure occurs near the center of the rollers, and the area where roller pressure is zero on the transmission side decreases. When positive and negative bending forces are applied to the operating and transmission sides, respectively, the imbalance in roller pressure is exacerbated. The transition zone between the operating and transmission sides is defined by the center of the rolls. On the operating side, the roller pressure increases rapidly, averaging 25 MPa under a non-symmetric bending force of 30 MPa. Conversely, on the transmission side, there is a slight decrease in roller pressure, and the number of areas where the roller pressure is zero increases. From the analysis above, it can be concluded that applying asymmetric bending forces significantly impacts changes in roller pressure. In practical engineering applications, excessive bending forces should be avoided to prevent unbalanced roller pressure, which may damage the rolls.

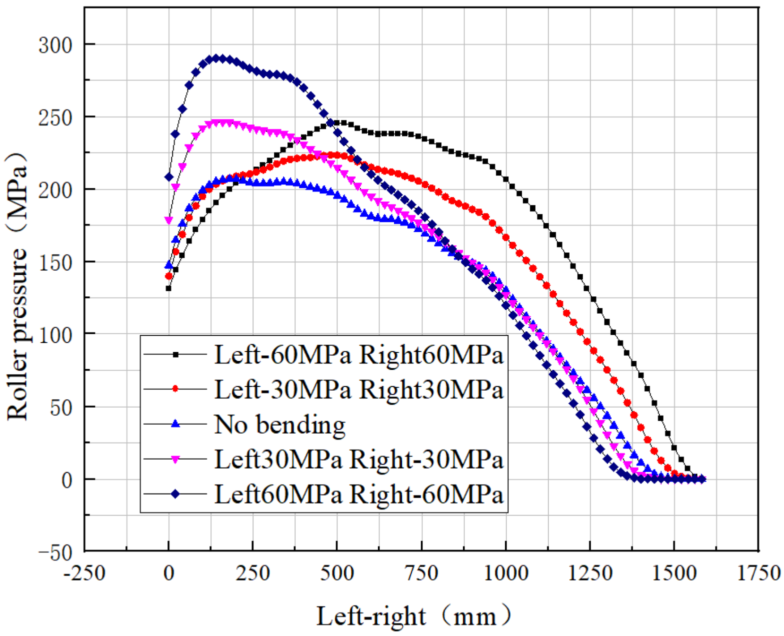

Figure 11. Horizontal distribution chart of inter-roller and support-roller pressures.

3.4. The Impact of Asymmetric Bending Force on the Thickness of the Steel Strip

An analysis of Figure 12 indicates that, in the absence of bending rolls, fluctuations in rolling forces at both ends of the mill result in a steel strip that is thinner on the left side compared to the right, with the center serving as the dividing line. This leads to a phenomenon where the thickness of the steel strip is greater on the right than on the left. As the non-symmetric bending force gradually increases, the change in thickness within 100 mm of the center remains relatively small, while significant changes occur on either side. Specifically, the thickness of the steel strip on the transmission side, influenced by positive bending rolls, increases, whereas the thickness on the operating side, affected by negative bending rolls, decreases. This results in a growing disparity in thickness between the two sides.

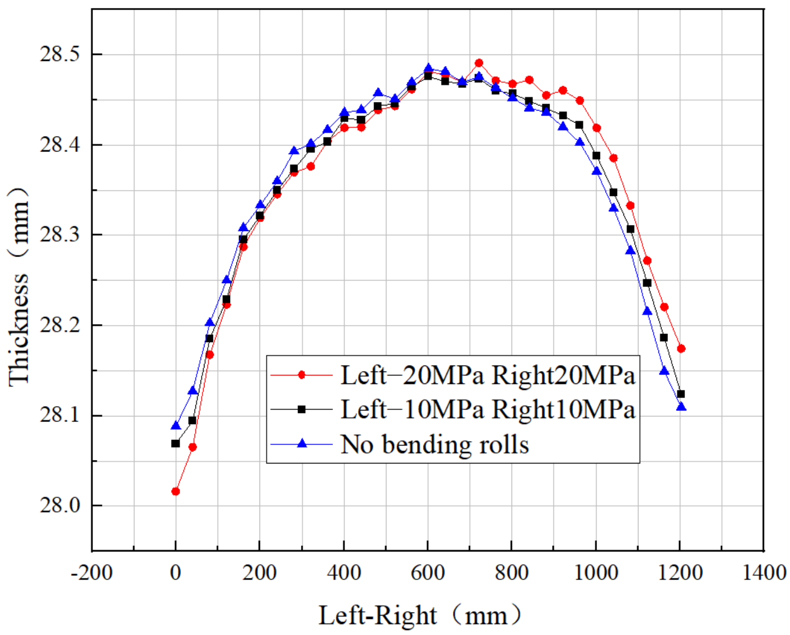

Figure 12. Strip transverse thickness distribution diagram with negative bending roll on the operating side and positive bending roll on the drive side.

This paper presents a set of simulation results that contrast with those depicted in Figure 12, where positive bending rolls are applied on the operating side, and negative bending rolls are applied on the transmission side. An analysis of Figure 13 reveals that when a positive bending roll of 10 MPa is applied on the operating side and a negative bending roll of 10 MPa is applied on the transmission side, the steel strip transitions from a left-thick, right-thin state to a relatively balanced thickness on both sides. However, as the non-symmetric bending force increases to 20 MPa, the steel strip once again exhibits a left-thick, right-thin trend. Therefore, when the phenomenon of unequal thickness on both sides of the steel strip occurs during the rolling process, a negative bending force can be applied to the thicker side, while a positive bending force of the same absolute value can be applied to the thinner side to address the issue of unbalanced shape.

3.5. The Impact of Asymmetric Bending Forces on the Crown and Edge Drop of the Steel Strip

As illustrated in Figure 12, the asymmetry of the bending force affecting the thickness of the steel strip results in significant differences in crown and edge drop between the operating and transmission sides of the strip. The calculation of crown and edge drop using the method of summing and averaging values from both sides does not accurately reflect the results. Therefore, it is essential to calculate the crown and edge drop of the steel strip on each side separately. For instance, the variation in thickness within 200 mm from the center of the steel strip on the operational side is relatively minor. However, beyond 300 mm from the center, the thickness of the metal strip decreases significantly, resulting in the formation of the edge thinning zone. Consequently, the difference between the thickness at the midpoint of the steel strip and the thickness 200 mm away from the center is defined as the steel strip's crown (C), while the difference between the thicknesses at 300 mm and 580 mm from the center is referred to as the steel strip's edge drop (E). The specific formulas for calculating the crown and edge drop of the steel strip are as follows:

$$C = h_i - h_j \quad (2)$$

In the formula, h_i is the thickness of the steel strip at its center, and h_j is the thickness of the metal strip 200 mm away from its center.

$$E = h_a - h_b \quad (3)$$

In the formula, h_a is the thickness of the metal strip 300 mm away from its center, and h_b is the thickness of the metal strip 580 mm away from its center.

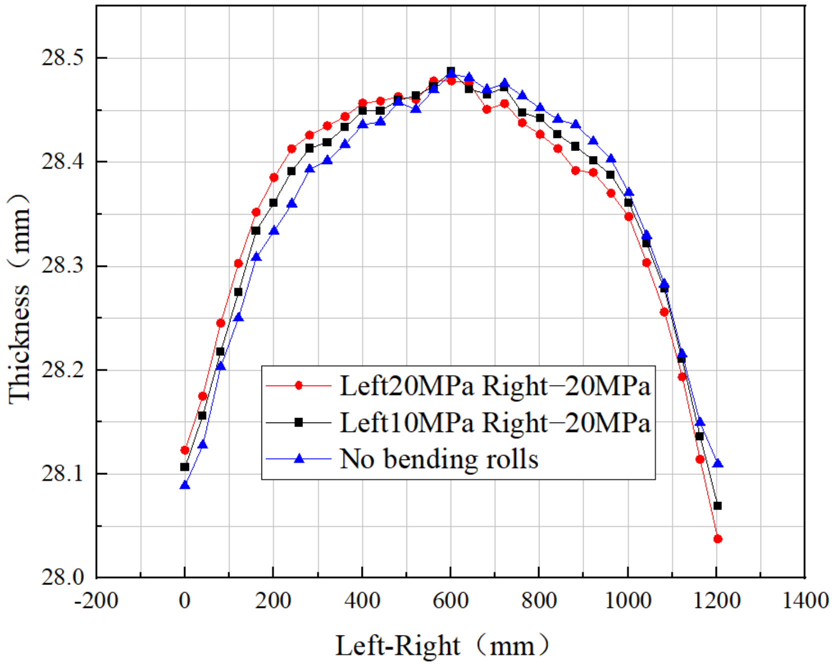

Figure 13. Strip transverse thickness distribution diagram with positive bending roll on the operating side and negative bending roll on the drive side.

As illustrated in Figure 14, both on the operational and transmission sides, the crown decreases with an increase in positive bending force and increases with an increase in negative bending force. Furthermore, there is a generally linear relationship between bending force and crown; adjusting the bending force by 1 MPa results in a change of 0.0009 mm in the crown of the metal strip. This text explains that when using asymmetric bending rolls to control the shape, applying force from the positive bending roll side helps reduce the crown of the metal strip and achieve better flatness. In contrast, using the negative bending roll side results in an increased crown and negatively impacts the flatness on one side of the metal strip. Analyzing Figure 15 reveals that the edge drop pattern on one side of the metal strip closely mirrors its crown change pattern; specifically, applying a positive bending force to one side alleviates the edge drop phenomenon while applying a negative bending force exacerbates it. Furthermore, the relationship between bending force and edge drop is linear; for every 1 MPa increase in bending force, there is a corresponding 0.001 mm change in edge drop. Therefore, when the edge drop phenomenon on one side of the metal strip is significant, the asymmetric bending force from a unilateral positive bending roll can be employed to regulate the shape.

3.6. The Impact of Asymmetric Bending Rolls on the Flatness of the Strip

The flatness of metal strips, also referred to as planarity, indicates the degree of arching before and after the rolling process. To analyze the impact of asymmetric bending rolls on the flatness of metal strips, this paper establishes the spatial coordinates along the width of the metal strips post-rolling. It translates all curve midpoints to a common point for a clearer comparison of the influence of non-symmetrical bending forces on metal strip flatness. In Figure 16, the variable X represents the coordinate of the metal strip along the width, while Y denotes the coordinate of the metal strip in the thickness direction, both measured in millimeters. Figure 16 illustrates the varying degrees of arching of the metal strip in the width direction under different conditions of non-symmetrical bending. Analyzing Figure 16 reveals that as the force of the asymmetric bending roll increases from 5 MPa to 20 MPa, the left end of the metal strip bends downward by approximately 0.0729 mm, while the right end bends upward by about 0.06076 mm. The nature of the shape defects in the metal strip gradually transitions from a near-sine wave to an edge wave. Consequently, the asymmetric bending role exerts a non-symmetrical control function over the shape. It can be inferred that when unilateral edge waves manifest in the metal strip, appropriate asymmetric bending forces can be employed to manage the transformation of the metal strip's shape from edge waves to sinusoidal waves. This shape can then be further adjusted through symmetric bending forces or other methods to correct the sinusoidal waves.

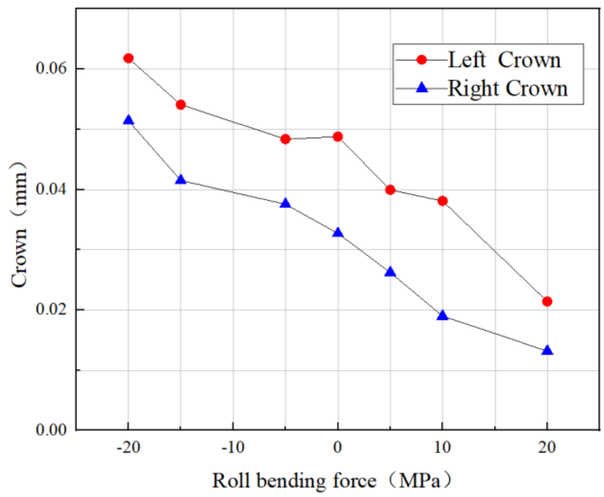

Figure 14. Bending force-crown diagram.

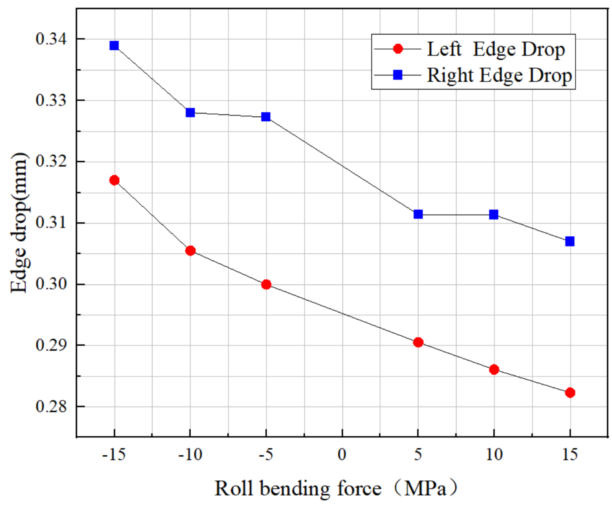

Figure 15. Roll bending force-edge drop diagram.

3.7. The Impact of Asymmetric Bending Forces on Their Controlling Effect

The coefficient of control effectiveness evaluates the ability of asymmetric bending forces to correct shape defects. The formula for the control effectiveness coefficient is as follows:

$$M = \frac{\triangle Y}{\triangle X} \tag{4}$$

In the formula, M represents the coefficient of control effectiveness, with units of mm/MPa; ΔY refers to the change in shape due to bending force adjustment; and ΔX refers to the adjustment quantity of bending force.

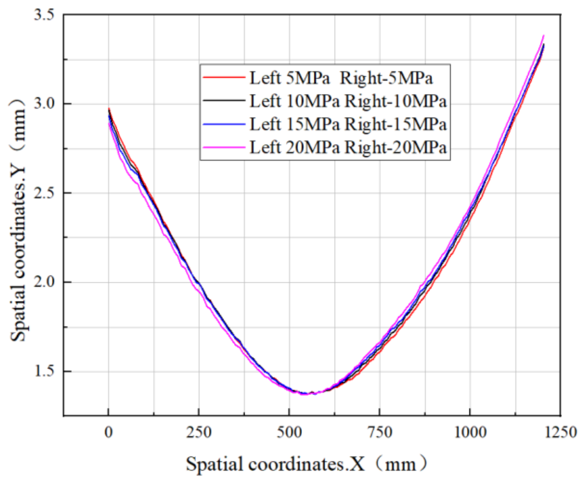

Figure 16. Metal strip flatness graph.

This article employs this formula as its foundation, selecting 121 points along the width of the steel strip. It calculates the coefficient of control effectiveness for non-symmetric bending at each point and analyzes the capacity of non-symmetric bending to regulate shape.

The function of bending roll adjustment is illustrated in Figure 17, where a negative bending roll force of 10 MPa is applied on the operating side, and a positive bending roll force of 10 MPa is applied on the transmission side. An analysis of Figure 16 reveals that the control effectiveness of bending rolls is significantly asymmetrical when non-symmetric bending forces are applied. The control effect on the edges of the strip is most pronounced, gradually decreasing as it moves toward the center of the strip, ultimately becoming zero at the horizontal axis of the strip. This indicates that asymmetric bending rolls can effectively control edge wave defects in strips without impacting their thickness.

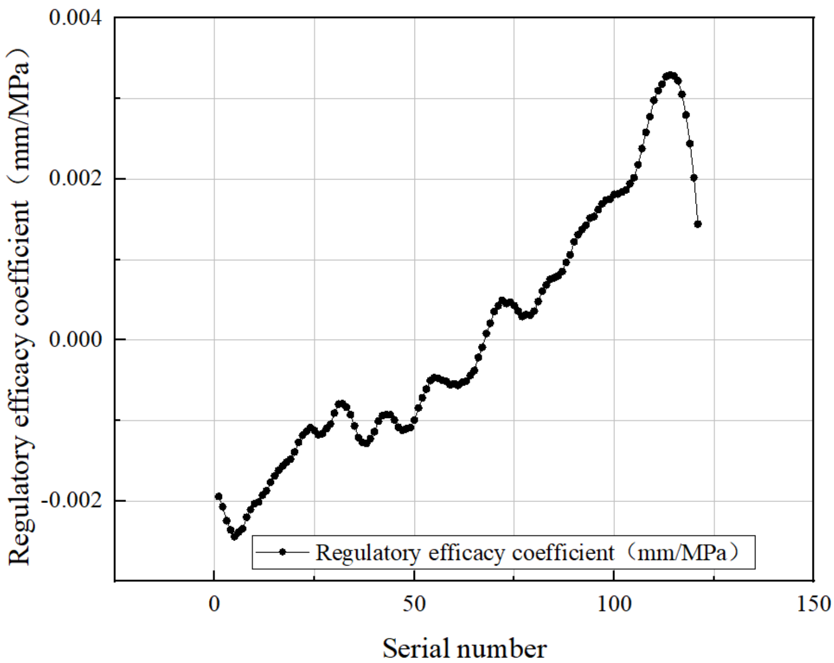

Figure 17. Diagram of regulatory efficacy of asymmetrical bending rolls.

To analyze the impact of the magnitude of asymmetric bending force on the control coefficient, this paper presents curves depicting the control coefficient at various magnitudes of asymmetric bending force. However, due to the instability of the rolling process, the curves of the control coefficient exhibit fluctuations of varying degrees. When these fluctuations are removed, the curves appear to be approximately linear. Consequently, this paper conducts linear fitting on the control coefficient curves. As illustrated in Figure 18, these are the fitted curves of the control coefficient at different non-symmetric bending forces. Analyzing Figure 18 reveals that the fitted curves of the control coefficient for different non-symmetric bending forces overlap significantly. The edge control efficiency coefficient for hot-rolled steel is approximately 0.002 mm/MPa, while the center control efficiency coefficient is roughly 0 mm/MPa. The greater the curvature slope, the larger the difference in shape control between the center and the edges, resulting in a higher effectiveness of bending roll force regulation. When the non-symmetric bending force is ±5 MPa, the slope of the curve is −0.000032; when the non-symmetric bending force is ±10 MPa, the slope of the curve is −0.000036; and when the non-symmetric bending force is ±20 MPa, the slope of the curve is −0.000038. This indicates that an appropriate increase in the non-symmetric bending force can enhance the control coefficient; however, the enhancement is minimal, and the control coefficients for different non-symmetric bending forces are quite similar.

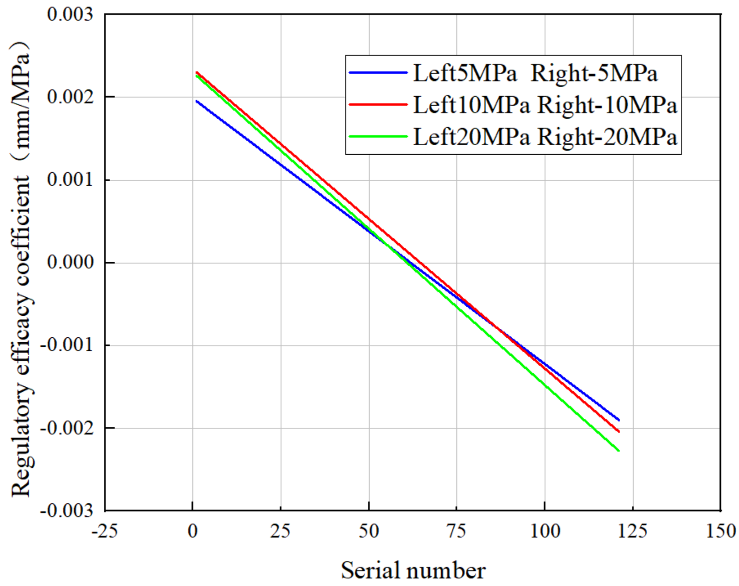

Figure 18. Fitting diagram of regulatory efficacy.

4. Conclusions

1. When steel strips are rolled using asymmetric bending rolls, the rolling pressure on the positive bending side is significantly reduced, while the rolling pressure on the negative bending side is slightly increased. This leads to non-uniform changes in strip thickness, with the thickness on the positive bending side increasing and the thickness on the negative bending side decreasing.
2. The shape of the rolled steel strip gradually transitions from a convex defect to a concave defect as the non-symmetrical bending force increases. Therefore, it can be concluded that when a unilateral concave shape defect occurs, an appropriate non-symmetrical bending force can be employed to correct the shape defect.
3. The inter-roller pressure in response to the non-symmetrical bending force exhibits an asymmetric change; specifically, the inter-roller pressure on the positive bending side increases while the inter-roller pressure on the negative bending side decreases.
4. During the rolling of steel strips using asymmetric bending rolls, the crown of the strips is influenced by the respective bending rolls, resulting in a linear relationship between the change in the crown and the change in bending force. The crown on the positive bending side flattens, while the crown on the negative bending side becomes more pronounced. The patterns of edge drop and crown variation in strips during asymmetric bending roll processing are similar. Additionally, edge drop changes and

bending forces are also linearly related. The occurrence of edge drop on the positive bending side is diminished, whereas it is intensified on the negative bending side.
5. The regulatory effect of asymmetric bending rolls on strip thickness varies linearly across the width of the strip, and the regulatory coefficients for different asymmetric bending rolls are generally consistent.

Author Contributions: Conceptualization, Z.Y.; methodology, Z.Y., S.P., Y.T. and W.C.; software, Z.Y., S.P., Y.T. and W.C.; validation, Z.Y., S.P., Y.T. and W.C.; formal analysis, Z.Y., S.P., Y.T. and W.C.; investigation, Z.Y., S.P., Y.T. and W.C.; resources, Z.Y.; data curation, Z.Y., S.P., Y.T. and W.C.; writing—original draft preparation, Z.Y., S.P., Y.T. and W.C.; writing—review and editing, Z.Y., S.P., Y.T. and W.C.; visualization, Z.Y., S.P., Y.T. and W.C.; supervision, Z.Y.; project administration, Z.Y.; funding acquisition, Z.Y. All authors have read and agreed to the published version of the manuscript.

Funding: This study is financially supported by the Natural Science Foundation General Program in Jiangsu Provincial of China (No.: BK20241965) and the Innovation Fund General Project of Nanjing Institute of Technology (No.: CKJB202209).

Data Availability Statement: The original contributions presented in the study are included in the article, further inquiries can be directed to the corresponding author.

Conflicts of Interest: The authors declare no conflict of interest.

References

1. Liu, Y.; Lin, D.; Zhao, X. Study on mechanical parameters and strip steering of aluminium alloy JP1235 under the influence of mill tilt. *Mod. Manuf. Eng.* **2008**, *12*, 62–65. [CrossRef]
2. Benke, M.; Schweitzer, B.; Hlavacs, A.; Mertinger, V. Prediction of Earing of Cross-Rolled Al Sheets from {h00} Pole Figures. *Metals* **2020**, *10*, 192. [CrossRef]
3. Li, W. Roll wear model and effect of work roll shifting on roll wear in hot srip mill. *J. Wuhan Inst. Technol.* **2013**, *36*, 98–103.
4. Zhang, J.S. The application status of aluminum strip and sheet cold rolling multi-stage cooling board shape control. *Technol. Sci. Technol. Wind* **2020**, *21*, 6+15. [CrossRef]
5. Sheng, Q.; Ren, P.J.; Fu, Q.K.; Dong, Y.Y.; Qu, X.D.; Wang, J. Research on the optimization of high-strength steel bending roller control process. *Metall. Equip.* **2023**, *S2*, 1–5+57.
6. Byon, S.M.; Roh, Y.H.; Yang, Z.R.; Lee, Y.S. A roll-bending approach to suppress the edge cracking of silicon steel in the cold rolling process. *Proc. Inst. Mech. Eng. Part B J. Eng. Manuf.* **2020**, *235*, 112–124. [CrossRef]
7. Stone, M.D.; Gray, R. Theory and practical aspects in crown control. *Iron Steel Eng.* **1965**, *8*, 73–90.
8. Shohet, K.N.; Townsend, N.A. Roll bending methods of crown control in four-high plate mills. *J. Iron Steel Inst.* **1968**, *11*, 1088–1098.
9. Fleck, N.; Johnson, K.; Mear, M.; Zhang, L.C. Cold rolling of foil. *Proc. Inst. Mech. Eng. Part B J. Eng. Manuf.* **1992**, *206*, 119–131. [CrossRef]
10. Kihara, J.; Peng, M.X. Application of BEM to Calculation of the Work Roll Deformation and Residual Stress in the Rolled Sheet. In *Boundary Elements VIII*; Tanaka, M., Brebbia, C.A., Eds.; Springer: Berlin/Heidelberg, Germany, 1968; Volume 8. [CrossRef]
11. Wang, Q.L.; Li, X.; Hu, Y.J.; Sun, J. Numerical analysis of intermediate roll shifting-induced rigidity characteristics of UCM cold rolling mill. *Steel Res. Int.* **2018**, *89*, 1700454. [CrossRef]
12. Montemayor-de la Garza, K.; Zambrano-Robledo, P.d.C.; Zapata-Hernandez, O.J.; Leduc-Lezama, L.A. Finite Element Modeling of Hot Rolling of 1075 Carbon Steel Process with Variable Cross Section. *Materials* **2023**, *16*, 2. [CrossRef]
13. Pondaven, C.; Erzar, B.; Spadaccini, A.; Grion, M. Finite element modeling evaluation of a void closure criterion using a multi-scale approach during hot rolling. *Metall. Ital.* **2023**, *5*, 36–41. [CrossRef]
14. Tian, B.; Kleber, S.; Turk, C.; Tolliner, S.; Schneller, S.; Markiewicz., P. Quantitative evaluation of relative sliding between billets and rolls in hot rolling. *Metall. Ital.* **2023**, *5*, 24–28. [CrossRef]
15. Linghu, K.Z.; Jiang, Z.Y.; Zhao, J.W.; Li, F. 3D FEM analysis of strip shape during multi-pass rolling in a 6-high CVC cold rolling mill. *Int. J. Adv. Manuf. Technol.* **2014**, *74*, 1733–1745. [CrossRef]
16. Shahani, A.R.; Setayeshi, S.; Nodamaie, S.A.; Asadi, M.A.; Rezaie, S. Prediction of influence parameters on the hot rolling process using finite element method and neural network. *J. Mater. Process Technol.* **2009**, *209*, 1920–1935. [CrossRef]
17. Wang, R.; Yang, Q.; He, A.; Shao, J.; Bian, H.T. Strip shape control capability of hot wide strip rolling mills. *J. Univ. Sci. Technol. Beijing Miner. Metall. Mater.* **2008**, *15*, 91–95. [CrossRef]
18. Li, Y.L.; Cao, J.G.; Qiu, L.; Kong, N.; He, A.; Zhou, Y.Z. Effect of strip edge temperature drop of electrical steel on profile and flatness during hot rolling process. *Adv. Mech. Eng.* **2019**, *11*, 1687814019840471. [CrossRef]

19. Yan, Z.W.; Bu, H.N.; Li, H.; Hong, L. Numerical simulation analysis of the rolling process based on the particle swarm hybrid algorithm. *Ironmak. Steelmak.* **2023**, *50*, 1321–1330. [CrossRef]
20. Sun, W.; Chen, L.; He, A.; Liu, C.; Yuan, T.H.; Qiang, Y. Study on quarter-wave control of DP980 steel based on a bending force linear combination strategy. *Int. J. Adv. Manuf. Technol.* **2023**, *127*, 2881–2892. [CrossRef]
21. Li, X.; Wang, Q.L.; Zhang, F.Y.; Zhang, Y.F. Present status and future prospects of strip flatness control based on elastic-plastic finite element. *Steel Roll.* **2020**, *37*, 1–11. [CrossRef]
22. Xie, H.B.; Xiao, H.; Zhang, G.M.; Liu, J.C. Analysison rolling pressure distribution of strip with different reductions by rxplicit dynamic FEM. *Gangtie Yanjiu Xuebao (J. Iron Steel Res.)* **2002**, *14*, 33–35.
23. Wang, P.; Yan, Z.; Li, X.; Zhang, D.H.; Duan, S.W. Edge drop control of cold rolled silicon steel strip based on model predictive control. *J. Manuf. Process.* **2022**, *82*, 88–95. [CrossRef]
24. Yu, H.L.; Liu, X.H.; Zhao, X.M.; Kusaba, Y. FEM analysis for V–H rolling process by updating geometric method. *J. Mater. Process Technol.* **2006**, *180*, 323–327. [CrossRef]
25. Pan, C.G.; Zhao, C.X.; Chang, Q.M.; Zhou, J.L.; Wu, Q. Three-dimensional metal particle flow simulation during the whole rolling process for 60 kg/m heavy rail. *Adv. Mech. Eng.* **2017**, *9*, 1–19. [CrossRef]
26. Wang, Q.L.; Sun, J.; Li, X.; Wang, Z.H.; Wang, P.F.; Zhang, D.H. Analysis of lateral metal flow induced flatness deviations of rolled steel strip: Mathematical modeling and simulation experiments. *Appl. Math. Model.* **2020**, *77*, 289–308. [CrossRef]
27. Kapil, S.; Eberhard, P.; Dwivedy, S.K. Dynamic Analysis of Cold-Rolling Process Using the Finite-Element Method. *J. Manuf. Sci. Eng.-Trans. Asme* **2016**, *138*, 041002. [CrossRef]
28. Dasari, S.K.; Ganguly, S. Implementation of Experimental Static Recrystallization of High Strength Steel into Computational Simulation of Multi-pass Slab Hot Rolling. *Met. Mater. Int.* **2023**, *29*, 3340–3355. [CrossRef]
29. Sabar, S.K.; Patel, R.K.; Ghosh, S.K. Roll force prediction by combined FEM and ANN in the hot rolling process under nano-lubrication condition. *Int. J. Adv. Manuf. Technol.* **2024**, *134*, 3893–3904. [CrossRef]
30. Ji, Z.M.; Sun, K. Analysis and application of the work roll bending control system. *Shanxi Metall.* **2022**, *45*, 139–141. [CrossRef]
31. Jiang, X.Y.; Kang, Z.Q.; Li, Z.F.; Ma, Y.L. Analysis about the influence of bending roll force on plate shape of cold rolled sheet. *Inn. Mong. Sci. Technol. Univ. J.* **2013**, *32*, 148–151. [CrossRef]
32. Peng, W.J.; Peng, S.B.; Li, M.G.; Xu, H.; Liu, D. Effect of bending force and roll-shift on strip shape. *Wuhan Inst. Eng. J.* **2020**, *42*, 351–354. [CrossRef]
33. Zhang, Z.Q.; Li, H.J.; Huang, Q.X.; Jia, Z.H. The finite element analysis on the impact of bending force on the flatness of strips. *Shanxi Metall.* **2012**, *35*, 8–10+53. [CrossRef]
34. Zhang, G.Q. *The Simulation Study on the Influence of Cold Rolling Hydraulic Bending Force on the Board Shape*; Liaoning Technical University: Fuxin, China, 2008.
35. Shi, X.; Liu, X.H.; Wang, G.D.; Li, Q.S.; Xu, J.Y. FEM Analysis of Effect of Bending Force on the Crown of Strip. *Steel Roll.* **2006**, *3*, 10–13. [CrossRef]
36. Ma, C.; Zhang, G.Q.; Zhao, D.H.; He, T.Q.; Shang, R. Studies on Numerical Simulation of the Inflections of Bending Force for Strip Profile in Cold Rolling. *Angang Technol.* **2009**, *5*, 36–40.
37. Liu, B.Q.; Zhang, H.; Wang, Z.D.; Wang, J.S.; Zhang, Y. Theoretical research and application of the asymmetrical bending of work rolls for shape control in a cold rolling mill. *J. Beijing Technol. Bus. Univ.* **2012**, *34*, 184–189. [CrossRef]
38. Hu, D.Z.; Han, W.; Guo, R.; Li, Y.J. The influence of the bending roller mechanism of the heavy plate leveller on the stress of the rollers. *Metall. Equip.* **2024**, *2*, 53–56+41.
39. Liu, J.W.; Wen, J.G.; Wang, Y.; Zhang, L.; Sun, X.L. FEM analysis for asymmetric bending roll of roll process in hour-high mill. In Proceedings of the Ninth Chinese Metallurgical Society Young Academic Conference, Beijing, China, 15–17 October 2018; The Chinese Society for Metals: Beijing, China, 2018; pp. 378–380. [CrossRef]
40. Liu, S.L.; Li, T.T.; Li, R.F.; Qi, K.; Liu, Z.G. A comparative study of microstructure and corrosion resistance in DP980 steel joints under different laser welding method. *J. Mater. Res. Technol.* **2023**, *27*, 3870–3880. [CrossRef]
41. Duan, T.T. *Special Properties Analysis of Shape Control for HC Mill Based on Asymmetrical Shifting and Bending Force*; Yanshan University: Qinhuangdao, China, 2010.
42. *DIN EN ISO 683-1:2018*; Heat-Treatable Steels, Alloy Steels and Free-Cutting Steels. European Committee for Standardization: Brussels, Belgium, 2018.
43. Plessier, A.; Del Pino, S.; Després, B. Implicit discretization of Lagrangian gas dynamics. *Esaim-Math. Model. Numer. Anal.* **2023**, *57*, 717–743. [CrossRef]
44. Namadchi, A.H.; Alamatian, J. Explicit dynamic analysis using Dynamic Relaxation method. *Comput. Struct.* **2016**, *175*, 91–99. [CrossRef]
45. Liu, J.X.; Han, J.T.; Zhang, Y.J. Research status of high speed steel for rolls. *Mater. Rep.* **2009**, *23*, 74–77.
46. Xian, D.X.; Zheng, X.Z.; Xu, H.Q.; Zhang, A.M.; Song, R.G.; Tang, L.D.; Wang, F.X.; Cheng, Y. The development of Q345B hot-rolled steel plates with improved performance. *Shandong Metall.* **2004**, *1*, 189–191. [CrossRef]
47. Shu, C.; Cheng, L.; Xu, Y. Parameter estimation of Johnson-Cook constitutive model. *Chin. J. Nonferrous Met.* **2020**, *30*, 1073–1083.

48. Singh, G.; Singh, P.K. Hot profiled rolling of C40 steel: Production variable's effect on rolling performance. *Mater. Manuf. Process.* **2023**, *39*, 871–891. [CrossRef]
49. Dong, F.; Germain, G. Determining the Johnson-Cook Constitutive Equation Material Parameters via Finite Element Analysis Method. *J. Shanghai Jiao Tong Univ.* **2011**, *45*, 1657–1660+1667. [CrossRef]